united nations
educational, scientific
and cultural
organization

international atomic
energy agency

the
abdus salam
international centre for theoretical physics

SMR.1348 - 7

SECOND EUROPEAN SUMMER SCHOOL on MICROSCOPIC QUANTUM MANY-BODY THEORIES and their APPLICATIONS

(3 - 14 September 2001)

METAL CLUSTERS THAT BEHAVE LIKE GIANT ATOMIC NUCLEI

T. Patrick MARTIN
Max-Planck-Institut fuer Festkorperforschung
Heisenberg - Strasse 1
70569 Stuttgart
GERMANY

EXPERIMENTAL ASPECTS OF METAL CLUSTERS

T.P. MARTIN

1 Introduction

It is not obvious that metal clusters should behave like atomic nuclei – but they do. Of course the energy and distance scales are quite different. But aside from this, the properties of these two forms of condensed matter are amazingly similar. The shell model developed by nuclear physicists describes very nicely the electronic properties of alkali metal clusters. The giant dipole resonances in the excitation spectra of nuclei have their analogue in the plasmon resonances of metal clusters. Finally, the droplet model describing the fission of unstable nuclei can be successively applied to the fragmentation of highly charged metal clusters. The similarity between clusters and nuclei is not accidental. Both systems consist of fermions moving, nearly freely, in a confined space.

Many years ago it was noticed that atomic nuclei containing either 8, 20, 50, 82 or 126 protons have very long lifetimes. It was a challenge for the nuclear physicists back in the forties to explain these so-called magic numbers. Since physicists tend to see most objects as perfectly round, it should come as no surprise that they assumed atomic nuclei are spherically symmetric. Under this assumption they had to solve only a radial Schrödinger equation.

$$\left[-\frac{d^1}{dr^2}+\frac{\ell(\ell+1)}{r^2}+V(r)\right]P_{n\ell}(r)=E_{n\ell}P_{n\ell}(r) \tag{1.1}$$

where ℓ is the angular momentum quantum number and V(r) is the radial dependence of the potential in which the nucleons move. They assumed further that the potential could be described by a simple potential well. Some confusion can arise because nuclear physicists and atomic physicists use slightly different definitions for the principal quantum number n,

$$\text{n(atomic)} = \text{n(nuclear)} + \ell \tag{1.2}$$

Throughout this lecture we will use the principal quantum number from nuclear physics, i.e., n denotes the number of extrema in the raidal wavefunction.

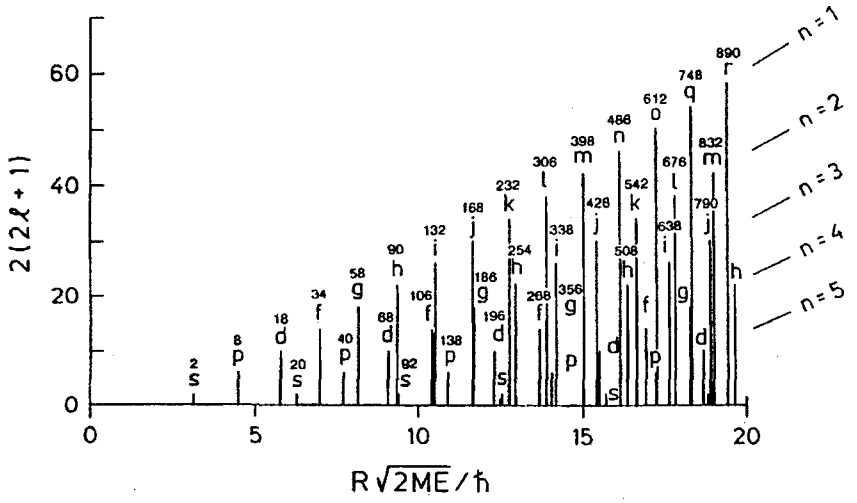

Fig. 1. The degeneracy of states of the infinitely deep spherical well on a momentum scale. The total number of fermions needed to fill all states up to and including a given subshell is indicated above each bar.

Eigenstates of the radial Schrödinger equation are often called subshells. The subshells of the infinite spherical potential well are shown ordered according to momentum in Fig. 1. The lowest energy state is 1s then comes 1p, 1d, 1f, 2p ..., etc. This is, with 2, 8, 18, 20, 34, 40, 58, 90 ... nucleons, subshells are completely filled and the corresponding nuclei could be expected to be exceptionally stable. However, these are not the observed magic numbers.

In 1949 Maria Goeppert-Mayer [1] and Haxel, Jensen and Suess [2] came up with a modified model which yielded the obseved magic numbers. Their idea was that the spin-orbit interaction is unusually strong for nucleons. Subshells with high angular momentum split and the states rearrange themselves into different groups. As we shall see the original shell model, which the nuclear physicist had to discard, describes very nicely the electronic states of metal clusters [3-18].

2 Subshells, Shells and Supershells

If it can be assumed that the electrons in metal clusters move in a spherically symmetric potential, the problem is greatly simplified. Subshells for large values of angular momentum can contain hundreds of electrons having the same energy. The highest possible degeneracy assuming cubic symmetry is only 6. So under spherical symmetry the multitude of electronic states condenses down into a few degenerate subshells. Each subshell is characterized

by a pair of quantum numbers n and ℓ. Under certain circumstances the subshells themselves condense into a smaller number of highly degenerate shells. The reason for the formation of shells out of subshells requires more explanation.

The concept of shells can be associated with a characteristic length. Every time the radius of a growing cluster increases by one unit of this characteristic length, a new shell is said to be added. The characteristic length for shells of atoms is approxiamtely equal to the interatomic distance. The characteristic length for shells of electrons is related to the wavelength of an electron in the highest occupied energy level (Fermi energy). For the alkali metals these lengths differ by a factor of about 2. This concept is useful only because the characteristic lengths are, to a first approximation, independent of cluster size.

The concept of shells can also be described in a different manner. An expansion of N, the total number of electrons, in terms of the shell index K will always have a leading term proportional to K^3. One power of K arises because we must sum over all shells up to K in order to obtain the total number of particles. One power of K arises because the number of subshells in a shell increases approximately linearly with shell index. Finally, the third power of K arises because the number of particles in the largest subshell also increases with shell index. Expressing this slightly more quantitatively, the total number of particles needed to fill all shells, k, up to and including K is

$$N_K = \sum_{k=1}^{K} \sum_{\ell=0}^{L(k)} 2(2\ell = 1) \sim K^3 \tag{2.1}$$

where L(k) is the highest angular momentum subshell in shell k.

Shell structure is not necessarily an approximate and infrequent bunching of states as in the example of the spherical potential well, Fig. 1. Clearly, almost none of the subshells occur exactly at the same energy for this potential. Shell structure can be the result of exactly overlapping states. Such degeneracies signal the presence of a symmetry higher than spherical symmetry. Subshells of hydrogen for which $n + \ell$ have the same value, have exactly the same energy. This additional degeneracy in the states of hydrogen is a result of the form of its potential, 1/r, which bestows on hydrogen 0(4) symmetry. Subshells of the spherical harmonic oscillator for which $2n + \ell$ have the same value also have exactly the same energy due to the form of the potential, r^2, and the resulting symmetry, SU(3). For this reason it is said that these systems, hydrogen and oscillator, have quantum numbers $n + \ell$ and $2n + \ell$ that determine the energy. We have shown that $3n + \ell$ is an approximate energy quantum number for alkali metal clusters [16]. As

the cluster increases in size, electron motion quantized in this way would finally be described as a closed triangular trajectory [19].

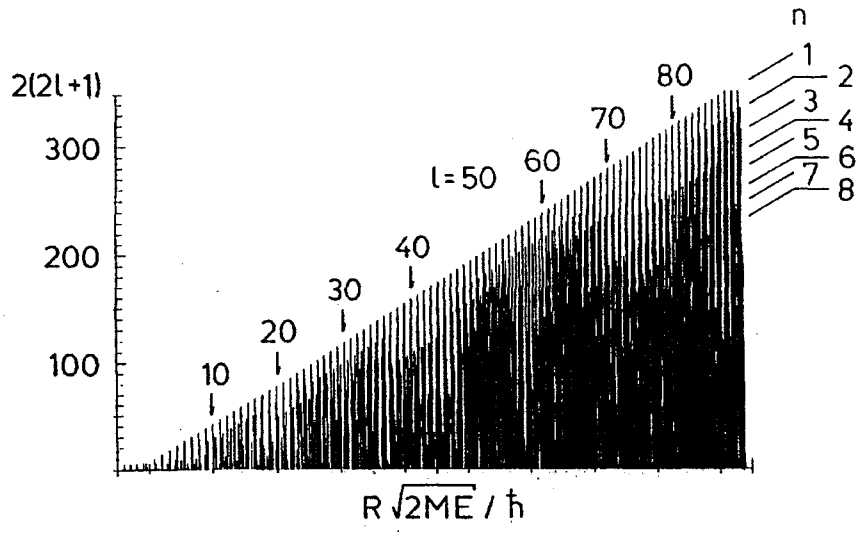

Fig. 2. The states of the infinitely deep sphereical well for very large values of ℓ. Notice the periodic bunching of states into shells. This periodic pattern is referred to as supershell structure.

The grouping of large subshells into shells is illustrated in Fig. 2 for the spherical potential well. Here, it can again be seen that in certain energy or momentum regions the subshells bunch together. However, the states are so densely packed in this figure that the effect is perceived as an alternating light-dark pattern. That is, for the infinite potential well, bunching of states occurs periodically on the momentum scale. The periodic appearance of shell structure is referred to as supershell structure [20,21]. Although supershell structure was predicted by nuclear physicists more than 15 years ago, it has never been observed in nuclei. The reason for this is very simple. The first supershell beat or interference occurs for a system containing 800 fermions. There exist, of course, no nuclei containing so many protons and neutrons. It is possible, however, to produce metal clusters containing such large numbers of electrons.

3 The Experiment

The technique we have used to study shell structure in metal clusters is photoionization time-of-flight (TOF) mass spectrometry, Fig. 3. The mass spectrometer has a mass range of 600 000 amu and a mass resolution of up to 20 000. The cluster source is a low-pressure, rare gas, condensation cell. Sodium vapor was quenched in cold He gas having a pressure of about 1

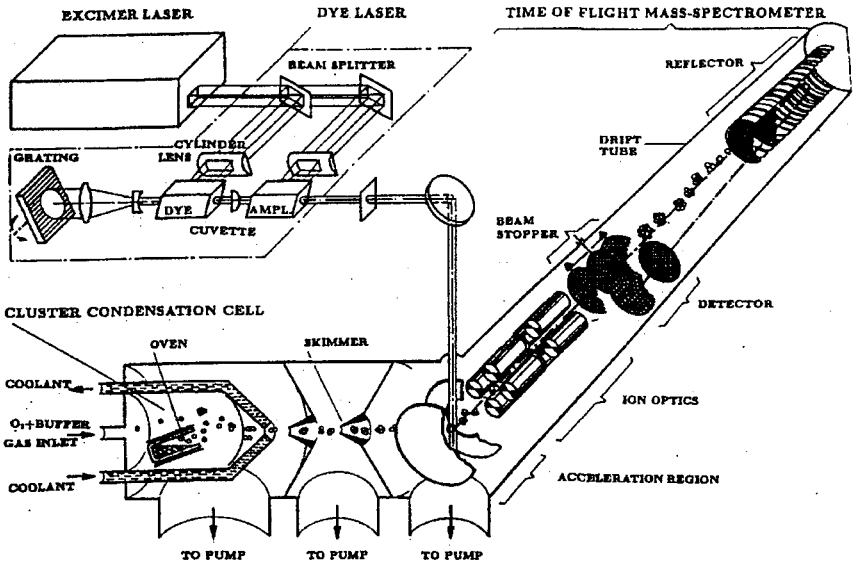

Fig. 3. Apparatus for the production, photoionization and time-of-flight mass analysis of metal clusters.

mbar. Clusters condensed out of the quenched vapor were transported by the gas stream through a nozzle and through two chambers of intermediate pressure into a high vacuum chamber. The size distribution of the clusters could be controlled by varying the oven-to-nozzle distance, the He gas pressure, and the oven temperature. The clusters were photoionized with a laser pulse.

Since phase space in the ion optics is anisotropically occupied at the moment of ionization, a quadrupole pair is used to focus the ions onto the detector. All ions in a volume of 1mm^3 that have less than 500 eV kinetic energy at the moment of ionization are focused onto the detector [22].

The reflector consists of two segments with highly homogeneous electric fields, separated by wire meshes. The first segment, which is twice completely traversed by the ions, is called the retarding field, and the other segment is called reflecting field. This two-stage reflector allows a second-order time focusing of ions [23]. Two channel plates in series are used to detect the ions. The secondary electrons are collected on a metal plate and conducted to the electronics. The following main design features of the instrument are necessary to achieve such a resolution [24]:

1. The ions are accelerated at right angles to the neutral cluster beam. If clusters are ionized by a laser pulse from the gas phase, there will always be a distribution of initial *potential* energies. The reflector is used to compensate for these. If the neutral beam is parallel to the acceleration direction, there is also an initial distribution of *kinetic*

energies or velocity components parallel to the acceleration diretion. If the reflector is used to compensate for the initial potential energy, it cannot also compensate for the kinetic energies.

2. A long (29cm) retarding field segment is used in the reflector. In the vicinity of the wire meshes at the end of the two reflector segments the electric field is not perfectly homogeneous. This causes a slight deflection of ions passing through them and thus a small time error. By using along retarding field segment, the field in he vicinity of the wire meshes is lowered, and the deflection of ions passing through them is reduced.

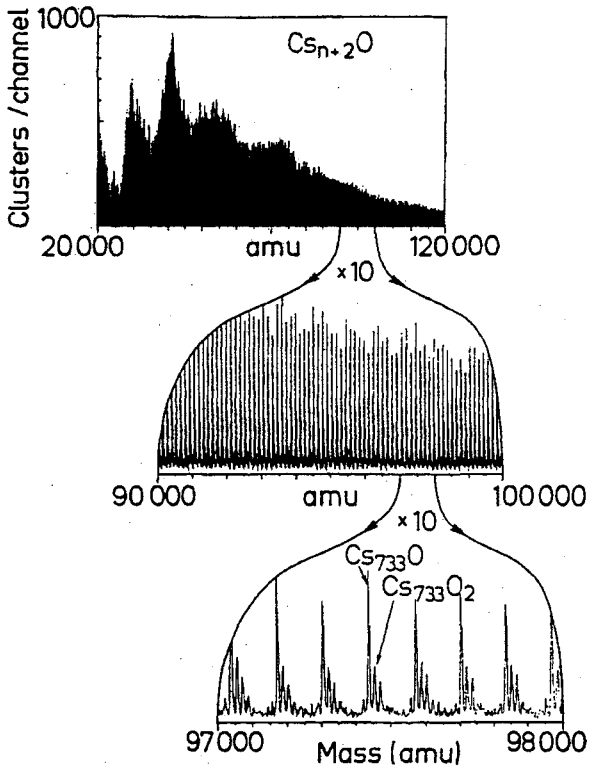

Fig. 4. Mass spectrum of Cs-O clusters.Notice that the exact composition can be determined on an expanded mass scale.

The mass spectra which will be displayed in this paper cover a large range of masses. For this reason it will not be possible to distinguish the individual mass peaks. For example, at the top of Fig. 4 we have reproduced a mass spectrum of Cs-O clusters which appears to be nothing more than

a black smudge. How do we know how many oxygen atoms th clusters contain? This can be seen by graphically expanding the scale by a factor of 100, Fig. 4. Because of the high resolution of our mass spectrometer, we are quite certain about the composition of the clusters examined.

4 Observation of Electronic Shell Structure

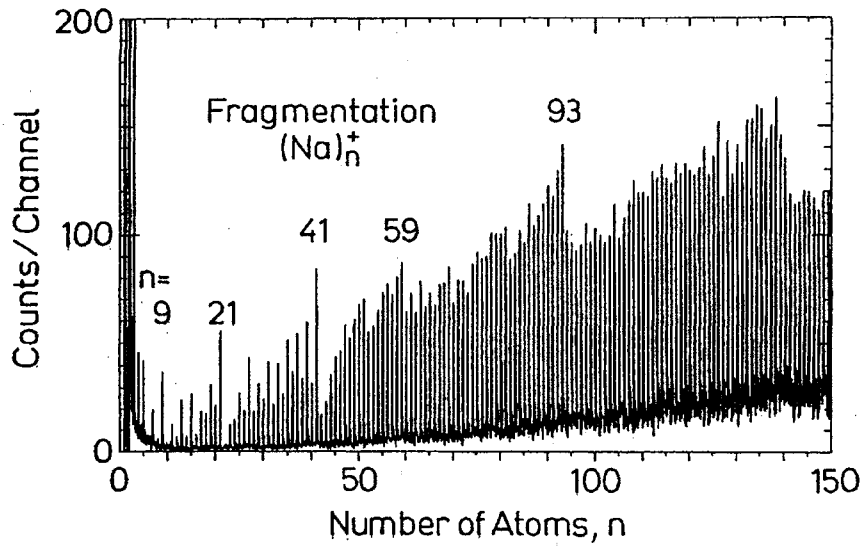

Fig. 5. Mass spectrum of $(Na)_n^+$ clusters ionized with high-intensity, 2.53 eV light. The clusters are fragmented by the ionizing laser. Fragments having closed-shell electronic configurations are particularly stable.

Knight, Clemenger, de Heer, Saunders, Chou and Cohen [3] first reported electronic shell structure in sodium clusters in 1984. Electronic shell structure can be demonstrated experimentally in several ways: as an abrupt decrease in the ionization energy with increasing cluster size, as an abrupt increase or an abrupt decrease in the intensity of peaks in mass spectra. The first type of experiment can be easily understood. Electrons in newly opened shells are less tightly bound, i.e., have lower ionization energies. However, considerable experimental effort is required to measure the ionization energy of even a single cluster. A complete photoionization spectrum must be obtained and very often an appropriate source of tunable light is simply not available. It is much easier to observe shell closings in photoionization, TOF mass spectra. However, depending upon the intensity and wavelength of the ionizing laser pulse, the new shell is announced by either an increase or a decrease in mass peak height.

For high laser intensities, multiple-photon processes cause the mass spectra to be less wavelength sensitive and also cause considerable fragmentation

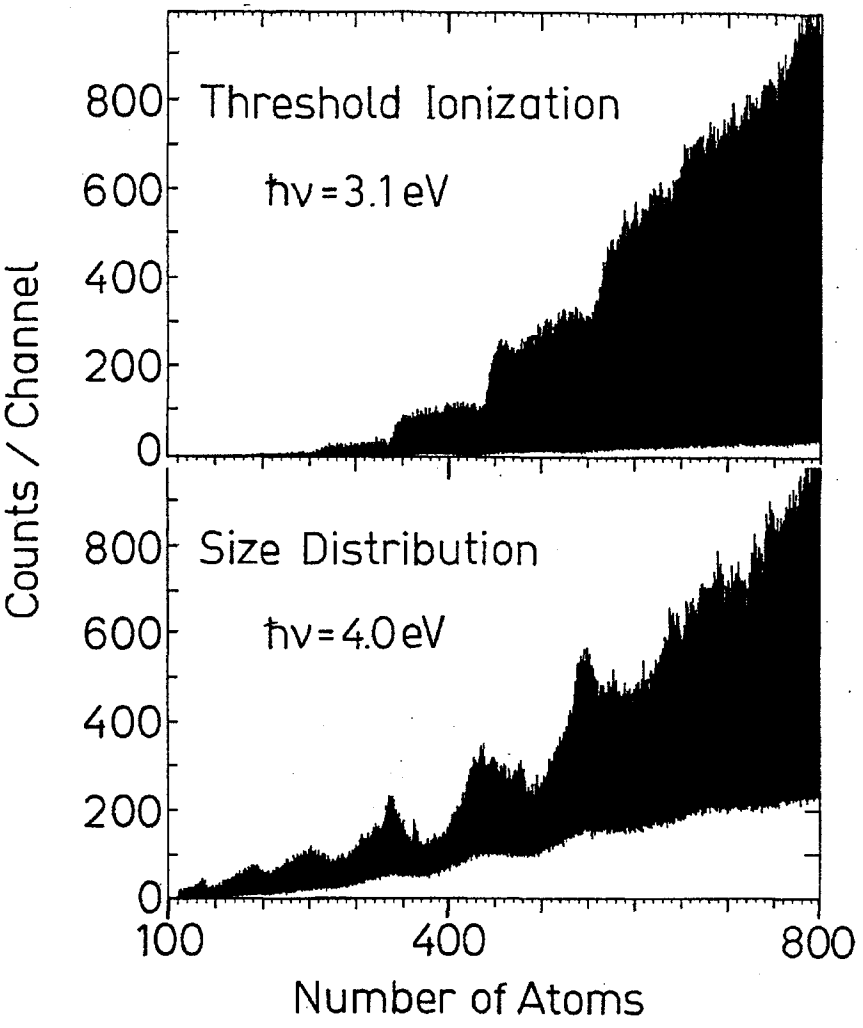

Fig. 6. Mass spectra of $(Na)_n$ clusters obtained using ionizing light near the ionization threshold (top) ($\hbar\nu = 3.1$ eV) and well above the ionization threshold (bottom) ($\hbar\nu-$ 4.0 eV). In both cases the neutral cluster beam was heated with 2.54 eV and 2.41 eV laser light.

of large clusters. The resulting mass spectrum reflects the stability of cluster ion fragments. Clusters with newly opened shells are less stable and are weakly represented in the mass spectra. Notice in Fig. 5 that as each new shell is opened there is a sharp step downward in the mass spectrum. Remember that cluster ions containing 9, 21, 41, 59, ... sodium atoms contain the magic number (8, 20, 40, 58, ...) of electrons.

For low laser fluence and wavelengths near the ionization threshold the mass spectra have a completely different character. As each new shell is

opened there is a sharp step upward in the mass spectra, Fig. 6 (top). Open shell clusters have low ionization thresholds which fall below the energy of the incident photons, while closed shell clusters remain unionized.

Finally, for low laser fluence and wavelengths well above the ionization threshold, it is possible to observe the neutral distribution of cluster sizes. If the source conditions are appropriately chosen, this distribution can peak at sizes corresponding to closed electronic shells, Fig. 6 (bottom).

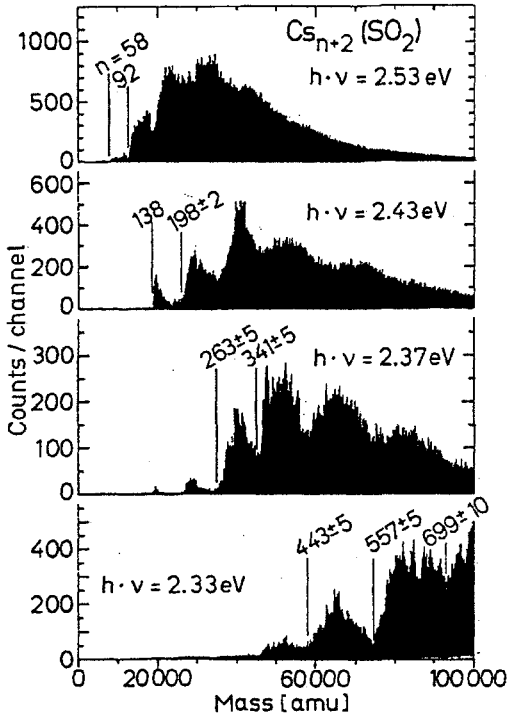

Fig. 7. Mass spectra of $Cs_{n+2}(SO_2)$ clusters with decreasing photon energy of the ionizaing laser from 2.53 eV (top) to 2.33 eV (bottom). The values of n at the steps in the mass spectra have been indicated (Ref.[15]).

Cluster intensities can sometimes be increased by a factor of ten by using a seed to nucleate the cluster growth. For example, by adding less than 0.02% SO_2 to the He cooling gas, Cs_2SO_2 molecules form which apparently promote further cluster growth. Mass spectra of $Cs_{n+2}(SO_2)$ clusters obtained [15] using four different dye-laser photon energies are shown in Fig. 7. Although it is not possible to distinguish the individual mass peaks in this condensed plot, it is evident that the spectra are characterized by steps. For example, a sharp increase in the mass-peak intensity occurs between n = 92 and 93. This can be more clearly seen if the mass scale is expanded by a factor of 50 (Fig. 8).

Notice also that the step occurs at the same value of n for clusters

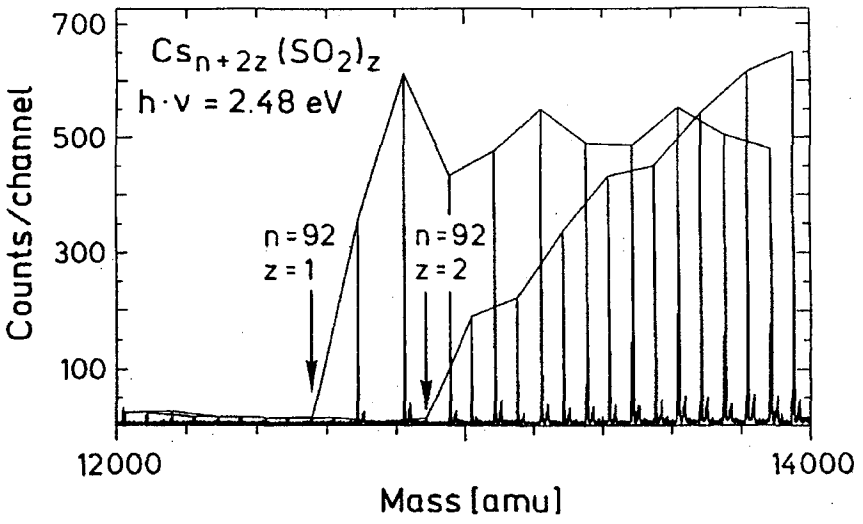

Fig. 8. Expanded mass spectra of $Cs_{n+2z}(SO_2)$ clusters for an ionizing photon energy of 2.48 eV. The lines connect mass peaks of clusters containing the same number z of SO_2 molecules. Notice that the steps for clusters containing (SO_2) and $(SO_2)_2$ are shifted by two Cs atoms (Ref.[15]).

containing both one and two SO_2 molecules. In addition to the steps for n = 58 and 92 in Fig. 7, there are broad minima in the 2.53 eV spectrum at about 140 and 200 Cs masses. These broad features become sharp steps if the ionizing photon energy is decreased to 2.43 eV. By successively decreasing the photon energy, steps can be observed for the magic numbers n = 58, 92, 138, 198±2, 263±5, 341±5, 443±5, and 557±5 [15, 17]. However, the steps become less well defined with increasing mass. We have studied the mass spectra of not only $Cs_{n+2}(SO_2)$ but also $Cs_{n+4}(SO_2)_2, Cs_{n+2}O$, and $Cs_{n+4}O_2$. They all show step-like features for the same values of n.

First, we would like to offer a qualitatiave explanation for these results and then support this explanation with detailed calculation. Each cesium atom contributes one delocalized electron which can move freely within the cluster. Each oxygen atom, and each SO_2 molecule, bonds with two of these electrons. Therefore, a cluster with composition $Cs_{n+2}(SO_2)$, for example, can be said to have n delocalized electrons. The potential in which the electrons move is nearly spherically symmetric, so that the states are characterized by a well-defined angular momentum. Therefore, the delocalized electrons occupy subshells of constant angular momentum which in turn condense into shells. When one of these shells is fully populated with electrons, the ionization energy is high and the clusters will not appear in mass spectra obtained using sufficiently low ionizing photon energy.

In other experiments [9] the closing of small subshells of angular mo-

mentum was shown to be accompanied by a sharp step in the ionization energy for Cs-O clusters having certain sizes, namely for $Cs_{n+2}O_z$ with n= 8, 18, 20, 34, 58 and 92. The closing at n = 40 seen in all other alkali-metal clusters could not be observed, neither in the experiments nor in the calculations. The steps were observed for clusters containing from one to seven oxygen atoms.

5 Density Functional Calculation

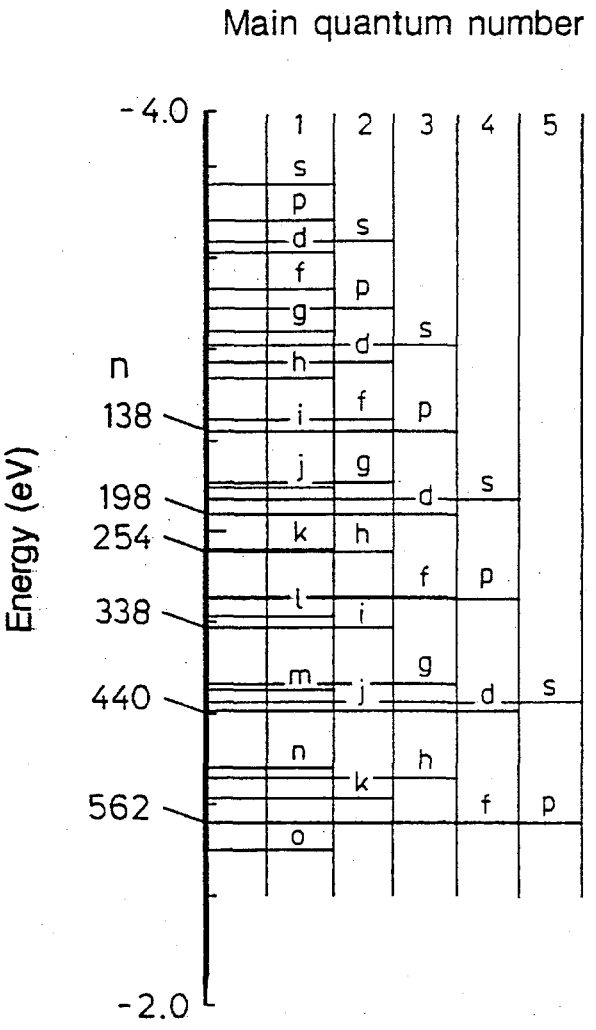

Fig. 9. The self-consistent, one-electron states of a 600 electron cesium cluster calculated using a modified spherical jellium background (Ref.[25]).

Self-consistent calculations have been carried out applying the density

functional approach to the spherical jellium model [10, 11]. We used an exchange correlation term of the Gunnarsson-Lundqvist form and a jellium density $r_S = 5.75$ corresponding to the bulk value of cesium. This model implies two improvements over the hard sphere model discussed earlier. Firstly, electron-electron interaction is included. Secondly, the jellium is regarded to be a more realistic simplification of the positive ion background than the hard sphere. The O^2 ion is taken into account only by omitting the cesium electrons presumably bound to oxygen. The calculations were performed on Cs_{600} clusters [25].

We found, that if a homogeneous jellium was used, the grouping of subshells was rather similar to the results of the infinite spherical potential well. However, a nonuniform jellium yielded a shell structure in better accordance to experimental results. We found that the subshells group fairly well into the observed shells only if the background charge distribution is slightly concentrated in the central region. This was achieved, for example, by adding a weak Gaussian (0.5% total charge density, half-width of 6 a.u.) charge distribtuion to the uniform distribution (width 48 a.u.). Figure 9 shows the ordering of subshells obtained from this potential. This leads to the rather surprising result that the Cs^+ cores seem to have higher density in the neighborhood of the center perhaps due to the existence of the O^{2-} ion. All attempts to lower the positive charge density in the central region led to an incorrect ordering of states.

The first calculation addressed the problem of the grouping of low-lying energy levels in one large Cs_{600} cluster. However, in the experiment the magic numbers were found by a rough examination of ionization potentials of the whole distribution of cluster sizes. A more direct way to explain magic numbers is to look for steps in the ionization potential curve of Cs–O clusters. Therefore, we calculated the ionization potentials of $Cs_{n+2}O$ For $n \leq 600$ and of $(Na)_n$ for $n \leq 1100$ using the same local-density scheme described above, Fig. 10. Starting from a known closed-shell configuration for n = 18, electrons were successively added. Three test configurations were calculated for each cluster size testing the opening of new subshells. The configuration with minimum total energy was chosen for the calculation of the ionization potential.

We found that the lower magic numbers n = 34, 58, 92 were well reproduced. For higher n distinct steps in the ionization potential were observed for n = 138, 196, 268, 338, 440, 562, 704, 854 and 1012. The absolute values of the calculated ionization potentials can be brought into better agreement with experiment by assuming that clusters have a 10–15% lower electron density than is fouond in the bulk. Magic number clusters exhibit unusually high ionization energies for the same reason rare gas atoms do: they possess a closed shell electronic configuration, Fig. 10. In this sense the metallic clusters behave like giant atoms.

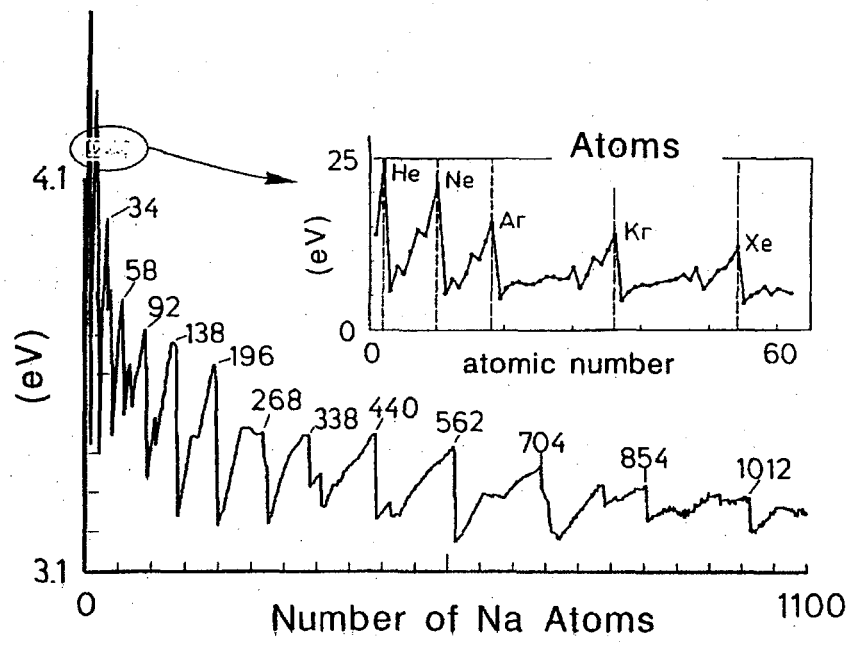

Fig. 10. Ionization potentials calculated as a function of n for $(Na)_n$ clusters. A positive background charge distribution slightly concentrated in the central region has been used. Notice the similar behavior of the ionization energies of the chemical elements (inset) (Ref.[25]).

6 Observation of Supershells

Although nuclear physicists speculated on the possible existence of supershells several decades ago, the phenomenon has never been observed in atomic nuclei for a very simple reason. No nucleus contains enough fermions to allow supershell formation. However, there is almost no limit to the number of electrons that can be contained in metal clusters.

Supershells are the periodic appearance and disappearance of shell structure in the energy density of states of a fermion system. In order to make clear the physical origin of supershells, it is necessary to go back one step to the semiclassical description of shells. Shells are associated with a charactristic length. Each time an integral number of fermi wavelengths fit into this length, a new shell has formed. The systems that we are studying are so large, that the classical picture of an electron bouncing back and forth inside a metal cluster is not completely without meaning. The characteristic length associated with a set of shells is just the length of a closed electron trajectory within the clusters. For spheres, two closed trajectories with almost the same length turn out to be the most important – a triangualr path and a square path. This leads to two sets with nearly the same energy

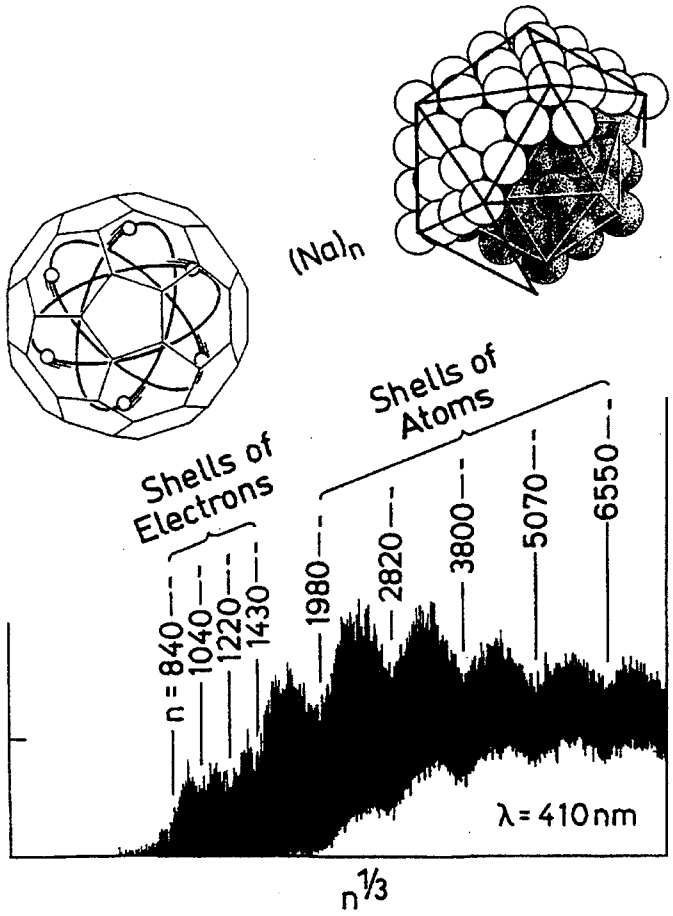

Fig. 11. Mass spectrum of $(Na)_n$ clusters photoionized with 3.02 eV photons. Two sequences of structures are observed at equally spaced intervals on the $n^{1/3}$ scale – an electronic shell sequence and a structural shell sequence.

spacing. These two contributions interfere with one another to produce a beat pattern known as quantal supershells. The first attempts to observe supershell structure in our laboratory were hindered by the unexpected appearance of a second set of shells in clusters containing more than 1500 atoms, Fig. 11.

These proved to be geometric shells of atoms that masked the weaker electronic shell structure. In the new experiments the geometric shell structure was surpressed by "melting" the clusters through heating with a continuous laser beam tuned to the plasmon frequency of the electron system.

The clusters wer warmed prior to ionization with a continuous Ar-ion laser beam running parallel to the neutral cluster beam. The laser light entred the ionization chamber through a heated window, passed through the

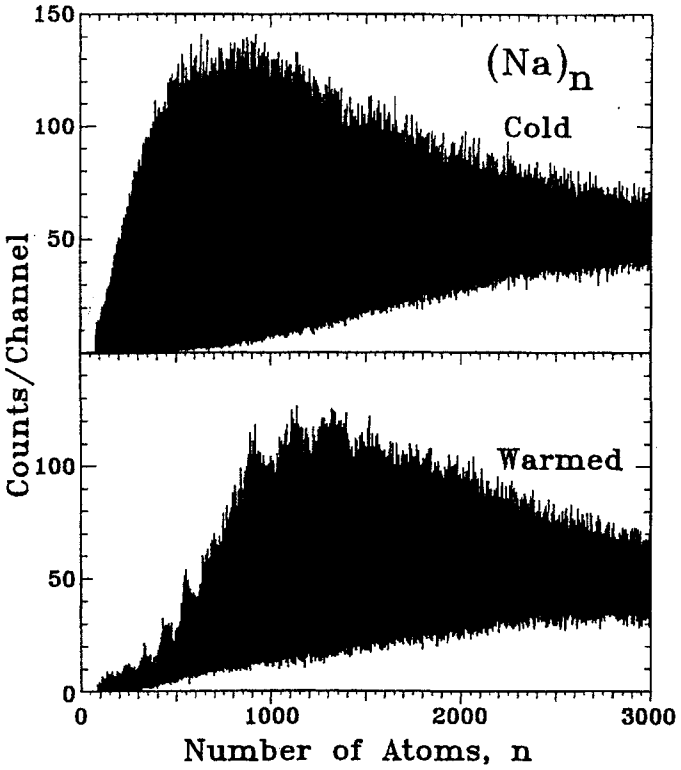

Fig. 12. Mass spectrum of $(Na)_n$ clusters using 4.0 eV ionizing light. The top spectrum shows the size distribution of cold clusters produced in the source; the bottom spectrum, after heating with 2.54 eV laser light.

ionization volume, through 2.2 mm Ø and 3.0 mm Ø skimmer aperatures, through a 3.0 mm nozzle, throught he oven chamber and finally exited through a second window where the laser intensity was recorded. Short wavelength light was found to warm much more efficiently. Using the 458 nm (2.71 eV) laser line, 10 mW proved sufficient to appreciable alter the neutral size distribution.

The size distribution obtained with ionizing photons having energy well above threshold are quite different from the spectra discussed in section 5 Without the warming laser the mass spectra are without structure, i.e. the size distribution of the cold clusters emerging from our source is smooth, Fig. 12. If the warming laser is turned on we obtain not steps but peaks as seen in the bottom of Fig. 12. We believe these peaks reflect the neutral size distribution of the laser-warmed clusters. It appears that it is usually possible to correlate a falling edge of the size disbribution with a step in the threshold ionization spectrum. Because of this correlation, we will characterize mass spectra obtained using excimer light by the number of atoms at steep negative slopes. A more extended mass spectrum of laser-warmed

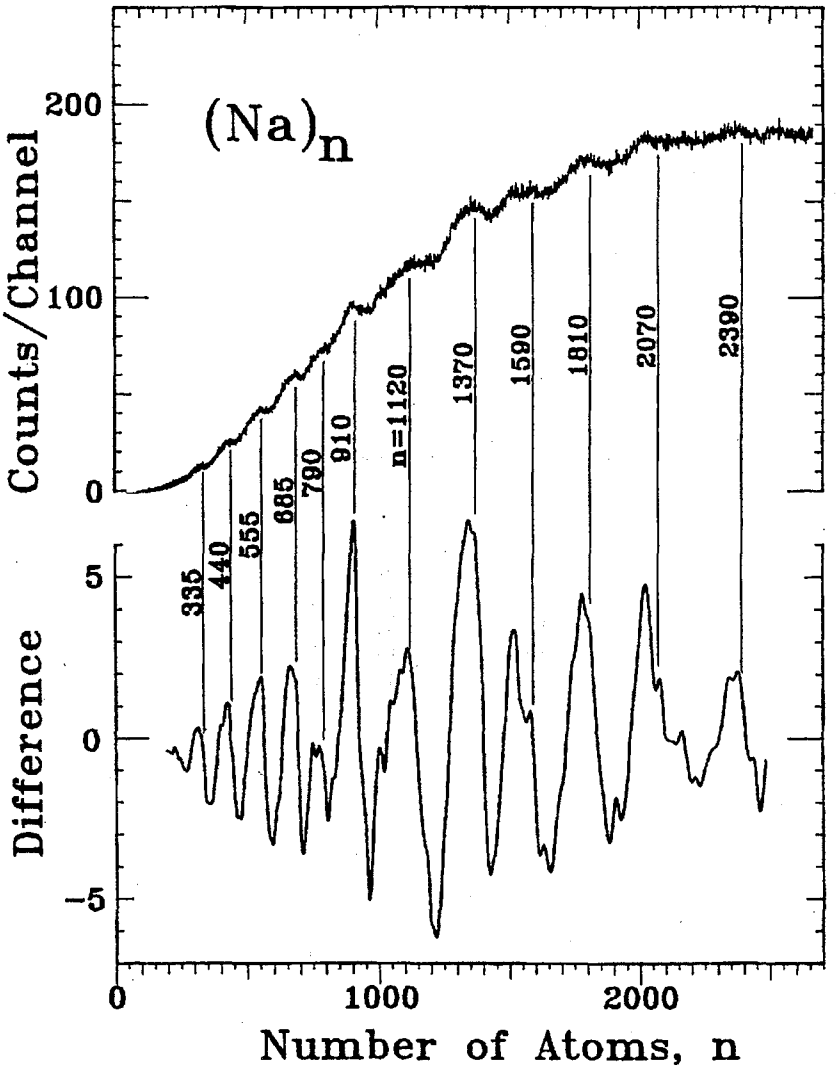

Fig. 13. Mass spectrum of $(Na)_n$ clusters using 4.0 eV ionizing light and (458nm) 2.71 eV continuous axial warming light having an intensity of 500 mW/cm^{-2}. The spectrum has been smoothed over one-hundred 16 ns time channels (top). In order to emphasize the shell structure an envelope function (obtained by smoothing over 20 000 time channels) is subtracted from a structural mass spectrum (smoothed over 1500 time channels). The difference is shown in the bottom spectrum.

sodium clusters obtained with 4.0 eV ionizing photons is shown at the top of Fig. 13. This spectrum has been smoothed with a spline function extending over one-hundred 16ns time channels. Notice that the structure observed does not occur at equal intrvals on a scale linear in mass. In order to present this structure in a form more convenient for analysis, the data have been

procesed in the following way. First, the raw data is averaged with a spline function extending over 20 000 time channels. The result is a smooth envelope curve containing no structure. Second, the raw data is averaged with a spline over 1500 channels. Finally, the two avearges are subtracted. The result is shown in the bottom of Fig. 13. Five independent measurements were made under the same experimental conditions. The positions, relative heights and widths of features in the mass spectra were well reproducible.

The clusters in this experiment have been warmed with a continuous laser beam running parallel to the neutral cluster beam. But what is implied by "warming"? consider the fate of a typical 500-atom cluster as it moves from the nozzle to the detector.

It leaves the nozzle with the temperature of the He carrier gas (~100K) traveling at a velocity of about 350 m/s. during its 1 ms flight to the ionization volume it undergoes no further collisions but does begint o absorb photons. We don't really know the absorption cross-section of this cluster at the warming laser wavelength (458nm). However, 1Å^2/atom is a typical upper limit for smaller clusters. It can be expected that the cross-section will be cluster size dependent. This size dependence will be reflected in the final mass distribution. The cluster absorbs the first 25 photons without evaporating any atoms, gaining an excess energy of about 70 eV and reaching a temperature of about 500 K. This all takes place in the first 450 μs. The temperture of the cluster remains rather constant for the last half of its journey to the ionization volume. It continues to absorb photons, of course, but after each absorption it evaporates 2 or 3 atoms returning to its original temperature before absorbing the next photon. It loses a total of 80 atoms, i.e. 16% of its original mass. It appears that this repeated heating and cooling through the "critical temperature for evaporation" on this time scale favors the evolution of a size distribution with relataively strong peaks near sizes corresponding to closed electronic shells.

The photon energy (4.0eV) of the ionizing laser has been chosen so that it is well above the ionization threshold (3.0 eV) of the sodium clusters investigated. The excess energy (1eV) insufficient to cause only one atom to evaporate. This is a neglibible loss on the mass scale we will be considering. For this reason, we believe that the magic numbers obtained reflect variations inthe size disbtribution of the neutral clusters induced by the warming laser.

The concept of shells can be associated with a characteristic length. Every time the radius of a growing cluster increases by one unit of this characteristic length, a new shell is said to be added. A good rough test of whether or not shell structure has been observed can be quickly carried out by plotting the shell index as a function of the radius or $n^{1/3}$. If the points fall on a straight line, the data is consistent with shell formation. That this is indeed the here, can be seen in Fig. 14. However, an even better fit can

be obtained using two straight lines with a break between shell 13 and 14. This too can be interpreted in an interesting way.

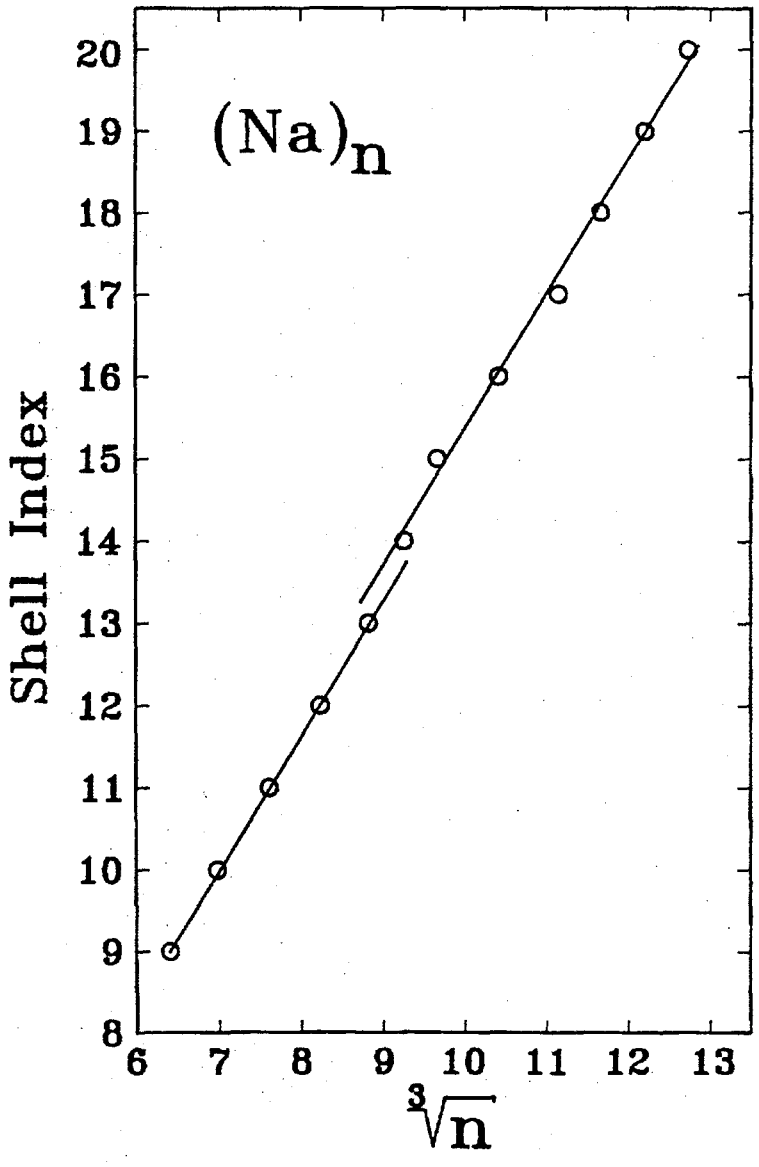

Fig. 14. The electronic shell closing falls approximately on a straight line if plotted on an $n^{1/3}$ scale. An even better fit is obtained using two straight lines with a break between shells 13 and 14. Such a break or "phase change" would be an indication of supershell structure.

It has been suggested [19-28] that shell structure might periodically appear and disappear with increasing cluster size. Such a supershell structure can be understood as a beating pattern created by the inteference of two

nearly equal periodic contributions. Quantum mechanically the contributions can be described as arising from competing energy quantum numbers. Classically, the contributions can be described as arising from two closed electron trajectories within a spherical cavity. One trajectory is triangular, the other square.

7 Fission

The fission of clusters was one of the first subjects [29-43] to be investigated in the newly developing field of cluster research. It is often referred to as Coulomb explosion, since the fission is caused by the Coulomb repulsion of like charges concentrated in a cluster smaller than a critical size. The kinetic energy that the charged fragments acquire can be as high as several eV. Most of these studies have delt with the fission of doubly or triply charged clusters. Recently we have shown that it is possible to induce charges as high as +14 on large Na clusters by photoionization [44]. In this section we will discuss fission in these highly charged clusters.

The technique we have used to study fission in sodium clusters is photoionization time-of-flight (TOF) mass spectroscopy. The cluster source is a low pressure, inert gas, condensation cell. The clusters were photoionized with a 50 mJ, 15ns, 193nm (6.4eV) excimer laser pulse focussed onto the neutral cluster beam with a 150 cm focal length quartz lens. The ionized clusters were heated 30 ns later with a second 5 mJ/mm^2, 470 nm (2.6eV) laser pulse.

The energy (I) required to remove an aditional electron from a cluster that already has charge +z can be written

$$I(z,R) = W + (\alpha + z)e^2/r \tag{7.1}$$

where W is the bulk work function, e is the electronic charge, and R is the radius of the cluster. Clearly, we have assumed that the cluster can be modelled as a conducting sphere. Various values of α have beenused in the literature. We will assume α is 0.5 and point out that for larg values of z the value of α used becomes unimportant. Since the radius of the cluster can be related to the number of electrons (or in our case atoms) through the Wigner-Seitz radius, $R^3 = r_s^3 n$, Eq. 4 can be rewritten as

$$I(z,n) = W + (\alpha + z)e^2/r_s n^{1/3}). \tag{7.2}$$

It can be seen from this expression that a larage amount of energy is required to remove electrons from small, highly charged clusters. If the amount of energy available is limited to that in one photon, then the maximum charge attainable for a cluster of a given size is

$$z_{max} = 1 - \alpha + (h\nu - W)r_s n^{1/3}/e^2. \tag{7.3}$$

This means that a two-dimensional cluster space (n,z) can be divided by a line into clusters that can be formed with, for example, an ArF excimer laser and those that cannot, Fig. 15. Also indicated in this figure is a line dividing the space into stable and unstable clusters. Notice that all of the values of n and z accessible with the ArF photons characterize stable clusters. The unstable clusters which we would like to investigate cannot be produced by direct multi-step ionization with this laser. There is, however, a way out of this dilemma.

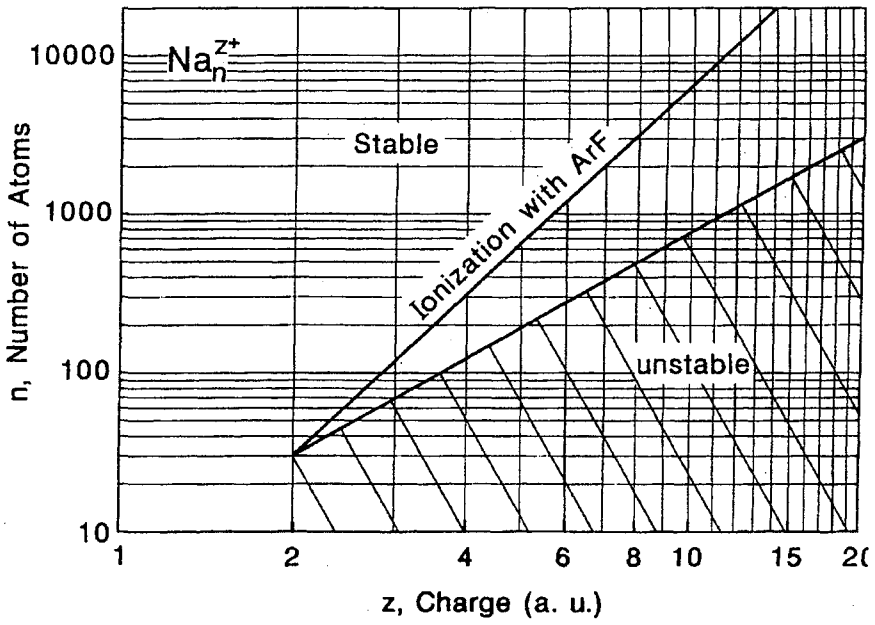

Fig. 15. The two-dimensional cluster space (n,z) can be divided by straight lines into Na_n^z clusters which can (cannot) be produced with an ArF laser and into clusters which are (are not) stable against Coulomb explosion. Notice that all clustrs (except for z = 2) that can be ionized with 6.4 eV photons are stable.

The ArF laser can be used to prepare a stable, highly charged, large cluster and then this large cluster can be reduced in size by heating and subsequent evaporation. A second laser pulse, containing photons with energies near the plasmon resonance of the sodium clusters, is used for heating. The clusters shrink down in size without charge until they reach a critical size at which they undergo fission. A mass spectrum, or better said, an n/z spectrum for Na_n^z clusters produced in this way is shown in Fig. 16. The log scale emphasizes, perhaps even overemphasizes, the effect we wish to show.

The highest set of mass peaks belongs to singly-charged sodium clusters. The peaks which occur exactly half-way between the Na_n^+ peaks are due to

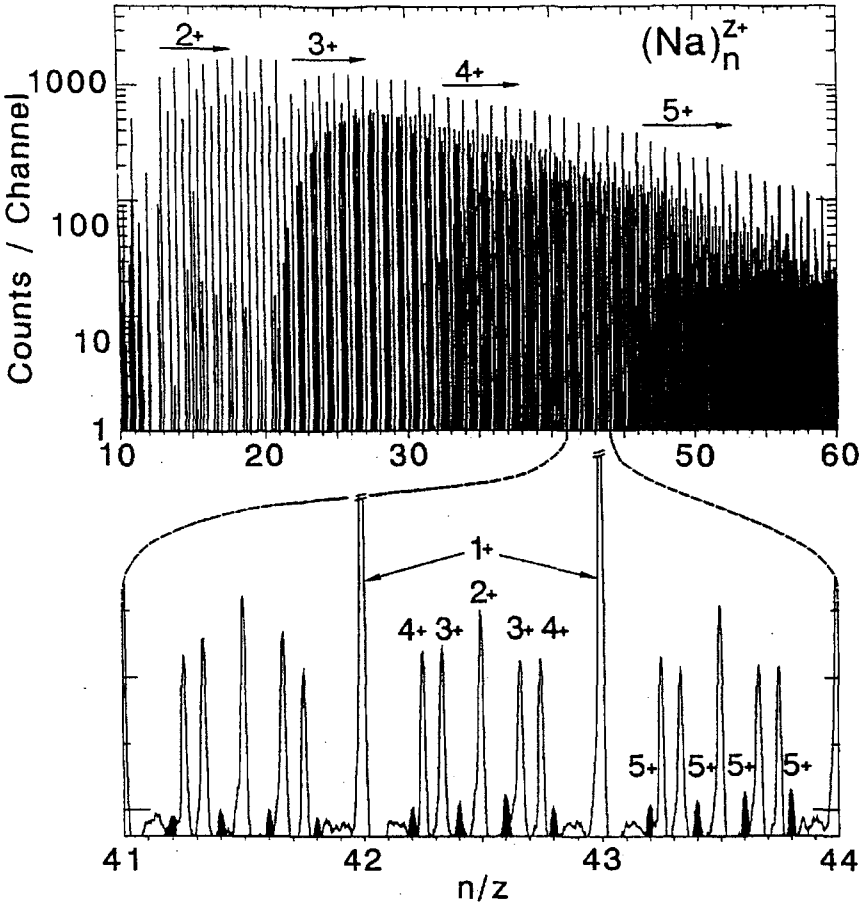

Fig. 16. An n/z spectrum of Na_n^z clusters. large clusters were first charged by multistep ionization using a high-fluence, arF laser. The clusters were then heated to reduce their size by evaporation. A portion of the spectrum is expanded to show the appearance threshold for Na_n^{5+} clusters (black filled).

Na_n^{2+} clusters. Notice that new sets of peaks appear in the spectrum at various critical values of n/z. This is perceived as a step-wise darkening of the mass spectrum. In the lower part of Fig. 16 we see the threshold region for the appearance of Na_n^{5+} on an expanded scale. Another segment of the spectrum on an expanded scale is shown in Fig. 17. This segment is near the threshold for the appearance of $Na^{6+}n$.

In this way, by careful examination of the fine structure in the mass spectra, it is possible to determine that the critical sizes for z = 1,2,3,4,5,6 and 7 are 27±1, 64±1, 123±2, 208±5, 321±5 and 448±10 atoms, respectively. These values are plotted on a double log scale in Fig. 18. They lie on a straight line with slope 2. This means that the critical condition for

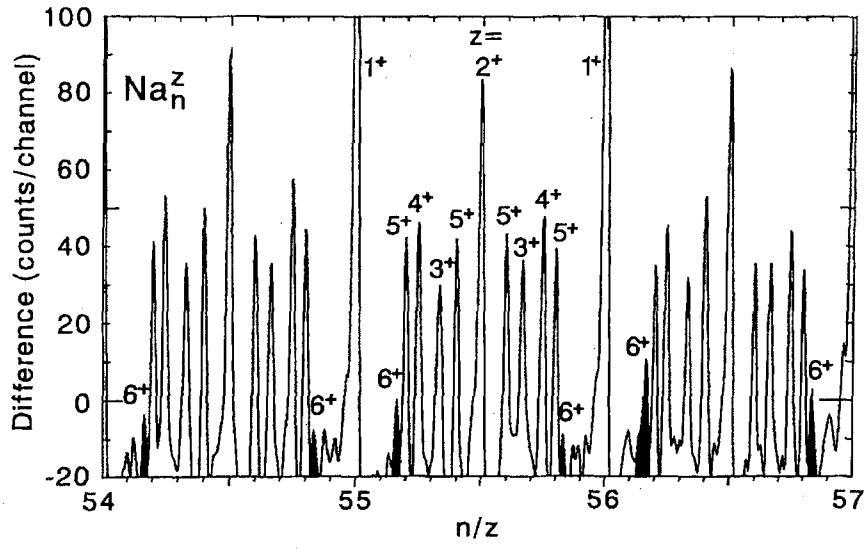

Fig. 17. An expanded portion of Fig. 16 showing the first appearance on Na_n^{6+} clusters. Smaller clusters in this charge state are not stable.

stability is

$$z^2/n \leq 0.125 \, . \tag{7.4}$$

z^2/n is proportional to the so-called fissility parameter used in nuclear phyciscs as a measure of stability. It has been shown inthe past that this parameter is also useful for clusters with small total charge [40, 41]. Here we see that it continues to be applicable for values of z up to 7.

The results of an extensive theoretical investigation of fission in Na clusters have recently been published [45, 46]. an important assumption made inthis work was that the fission is symmetric, i.e. the mass and charge of the original cluster are divided nearly equally between the fission productes. Unfortunately, we have no evidence at this time to either support or to challenge this assumption. Still, it is useful to compare the results of this calculation with our experiment, Fig. 18.

Here, cluster space (n,z) has been divided into stable metastable and unstable regions according to the tunneling criteria appropriate in nuclear physics. The fission process for nuclei can be described qualitatively in terms of three energies; the initial energy (E_i) of the charged, nondeformed clusters, the final energy (E_f) which is the sum of the energies of the noninteracting fission products. The third energy necessary to characterize fission products. The third energy necessary to characterize fission is the energy (E_b) of the lowest barrier separating the initial and final states. If $E_b < E_i$, the nucleus is unstable. If $E_f < E_i < E_b$, the nucleus is metastable to fission by tunneling through the barrier. Finally, if $E_f > E_i$, then the

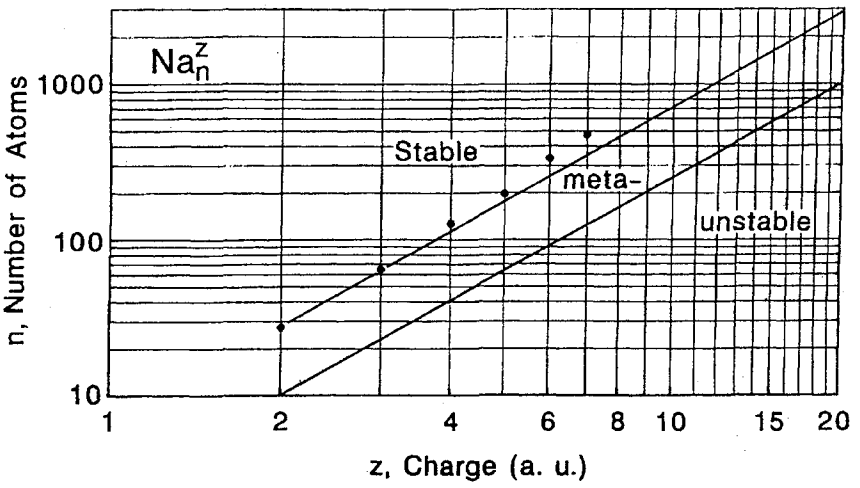

Fig. 18. The number of atoms in the smallest experimentally observed Na_n^z clusters (filled circles). The cluster space can be divided into stable, metastable and unstable regions, according to Ref. [45], using the symmetric liquid-drop model.

nucleus is stable. since tunneling for clusters has negligible probability, it is more accurate to say at zero temperature clusters are either stable or unstable, depending on whether there is a barrier or not. At finite temperature clusters can be classified as either unstable ($E_B < E_i$) or as metastable ($E_B > E_i$) to thermal hopping over the barrier. In practice it is useful to further subdivide the set of metastable clusters [36–38]. At finite temperatures clusters can lose mass and thermal energy by the evaporation of neutral atoms. Evaporation will always compete with fission and will, in fact, dominate if E_B is greater than E_v, the energy needed to evaporate an atom. For this reason, we have the conditions

a) unstable to fission, $E_B < E_i$;
b) metastable to fission, $E_i < E_B < E_v$; Since previous experiments [36–38] on doubly-charged Na and K clusters indicate that fission is strongly asymmetric, it would be appropriate now to consider this alternative. Even using the droplet model it is not easy to calculate the height of the barrier if the mass and charge can be distributed arbitrarily between the fission products. For this reason we will consider an energy which does not exactly characterize a real system, but it is trivial to calculate and therefore useful. It is the energy at the instant of scission, E_s. That is, starting from the final state we merely bring the fission products together until they just touch. Of course the energy increases monotonically from E_f to E_s according to Coulomb's Law. We assume that E_s is nearly equal to the barrier
c) metastable to evaporation, $E_i < E_v < E_B$.

height for the fission process. There is no unique value of E_s for a cluster in initial state n and z. Rather, a whole set of values exist corresponding to the various ways of distributing charge and mass between the fission products. However, one value of E_s has special significance and that is the minimum value. If this minimum value of $E_s < E_i$ the cluster is unstable and will spontaneously fission, even at zero temperature. If $E_s > E_i$ the cluster is stable against fission. Strictly speaking, one shuld say metastable because at finite temperatures the final state can be reached by jumping over the barrier, no matter how high. The results of these calculations are summarized

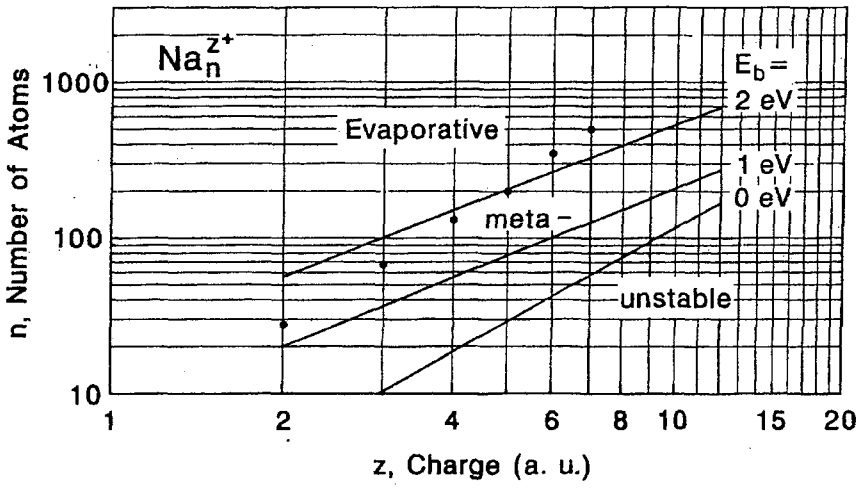

Fig. 19. Cluster space divided into evaporative and metastable und unstable regions. The barrier height has been obtained using an oversimplified model (see text). The number of atoms in the smallest experimentally observed Na_n^{z+} clusters is shown by the filled circles.

in Fig. 19. The initial and final energies are determined using the sphereical droplet model assuming only two fission fragments with arbitrary size and charge and assuming a surface tension parameter $\sigma = 200$ dyne/cm appropriate for sodium. One might expect that the experimental points would fall on the line corresponding to $E_B = E_V$. Clearly, this is not the case since E_v is known [36–38] to have a value of about 1 eV. That is, this rough model overestimates the barrier height by a factor of two. Various refinements are clearly needed; proper treatment of the Coulomb energy allowing for electron redistribution as the fragments move away from one another [48], a description of the asymmetric fission before scission, shell effects [49, 50] and entropy effects. Also needed are experiments demonstratinghow mass and charge are distributed between the fission fragments.

8 Concluding Remarks

Clearly, cluster science has greatly benefitted from the inspired work carried out by nuclear physicists decades ago. The shell model, the liquid droplet model, and the theory of giant dipole resonances have provided a ready and appropriate framework for understanding the properties of metal clusters. Hopefully, in the future, the exchange between nuclear science and cluster science will not be so one-sided, because metal clusters offer us a unique opportunity to study well-characterized, large fermion systems.

References

[1] Goeppert-Mayer, M. (1949) *Phys.Rev.* **75**, 1969L.

[2] Haxel, O., Jensen, J.H.D., Suess, H.E. (1949), **75**, 1766L.

[3] Knight, W.D., *et al.* (1984) *Phys. Rev. Lett.*

[4] Kappes, M.M., Kunz, R.W. Schumacher, E. (1982), *Chem. Phys. Lett.* **91**, 413.

[5] Katakuse, I., *et al.* (1985) *Int. J. Mass Spectrom. Ion Processes* **67**, 229.

[6] Bréchignac, C., Cahuzac, Ph., Roux, J.-Ph. (1986) *Chem. Phys. Lett.* **127**, 445.

[7] Begemann, W., *et al.* (1986) *Z. Phys.* **D3**, 183.

[8] Saunders, W.A., *et al.* (1986) *Phys. Rev.* **B32**, 1366.

[9] Bergmann, T., Limberger, H., Martin, T.P. (1988) *Phys. Rev. Lett.* **60**, 1767.

[10] Martins, J.L., Car, R., Buttet, J. (1981) *Surf. Sci.* **106**, 265.

[11] Ekardt, W., (1984) *Ber. Bunsenges. Phys. Chem.* **88**, 289.

[12] Clemenger, K. (1985) *Phys. Rev.* **B32**, 1359.

[13] Ishii, Y. Ohnishi, S., Sugano, S. (1986) *Phys. Rev.* **B33**, 5271.

[14] Bergmann, T., Limberger, H. (1989) *J. Chem. Phys.* **90**, 2848.

[15] Göhlich, H., *et al.* (1990) *Phys. Rev. Lett.* **65**, 748.

[16] Martin, T.P., *et al.* (1991) *Chem. Phys. Lett.* **72**, 209.

[17] Bjørnholm, S. ,*et al.* (1990) *Phys. Rev. Lett.*, **65**, 1627.

[18] Persson, J.L., *et al.* (1990) *Chem. Phys. Lett.*, **171**, 147; Honea, E.C., *et al.* (1990) *Chem. Phys. Lett.*, **171**, 147; Lerme, J., *et al.* (1992) *Phys. Rev. Lett.* **68**, 2818.

[19] Balian, R. and Bloch, C. (1971) *Ann. Phys.* **69**, 76.

[20] Bohr, A. and Mottelson, B.R. (1975) *Nuclear Structure* Benjamin, London).

[21] Nishioka, H., Hansen, K., Mottelson, B.R. (1990) *Phys. Rev.* **B42**, 9377.

[22] Bergmann, T. , *et al.* (1990) *Rev. Sci. Instrum.* **61**, 2585.

[23] Mamyrin, B.A., *et al.* (1973) *Sov. Phys. JETP* **37**, 45.

[24] Bergmann, T., Martin, T.P. and Schaber, H. (1990) *Rev. Sci. Instrum.* **61**, 2592.

[25] Lange, T. *et al.*, (1991) *Z. Phys. D* **19**, 113.

[26] Martin, T.P., *et al.* (1991) *Chem. Phys. Lett.* **186**, 53.

[27] Pedersen, J., *et al.* (1991) *Nature* **353**, 733.

[28] Bréchignac, C. *et al.* (1993) *Phys. Rev. B* **47**, 2271.

[29] Kreisle, D., *et al.* (1986) *Phys. Rev. Lett.* **56**, 1551.

[30] Echt, O. (1987) Physics and Chemistry of Small Clusters, P. Jena, B.K. Rao and S.N. Khanna (eds.), Plenun Press, New York.

[31] Echt, O. (1988) *et al.*, *Phys. Rev.* **A38**, 3236.

[32] Märk, T.D., *et al.* (1989) *Z. Phys.* **D12**, 279.

[33] Gotts, N.G., Lethbridge, P.G. and Stace, A.J. (1992) *J. Chem. Phys.* **96**, 408.
[34] Kandler, O, *et al.* (1991) *Z. Phys.* **D19**, 151.
[35] Sattler, K., *et al.* (1985) *Phys. Rev. Lett.* **47**, 160; Sattler, K. (1985) *Surf. Sci.* **156**, 292.
[36] Bréchignac, C., *et al.* (1990) *Phys. Rev. Lett.* **64**, 2893.
[37] Bréchignac, C., *et al.* (1991) *Z. Phys.* **D19**, 1.
[38] Bréchignac, C., *et al.* (1991) *Phys. Rev.* **B44**, 11386.
[39] Katakuse, I., Itoh, H., Ichihara, T. (1990) *Int. J. Mass. Spectrum. Ion Proc.* **97**, 47.
[40] Saunders, W.A. (1990) *Phys. Rev. Lett.* **64**, 3046.
[41] Saunders. W.A. (1991) *Z. Phys.* **D20**, 111.
[42] Schulze, W. (1987) *J. Chem. Phys.* **87**, 2402.
[43] Rabin, I., Jackschath, C. and W. Schulze (1991) *Z. Phys.* **D19**, 153.
[44] Näher, U. *et al.* (1992) *Phys. Rev. Lett.* **68**, 3416.
[45] Sugano, S. (1991) *Microcluster Physics*, Springer, Berlin, Heidelberg.
[46] Nakamura, M. *et al.* (1991) *Z. Phys.* **D19**, 145.
[47] Lipparini, E. and Vittori, A. (1990) *Z. Phys.* **D17**, 57.
[48] Garcias, F. *et al.* (1991) *Phys. Rev.* **B43**, 9459.
[49] Rao, B.K. *et al.* (1987) *Phys. Rev. Lett.* **58**, 1188.
[50] Barnett, R.N., Landman, U. and Rajagopal, G. (1991) *Phys. Rev. Lett.* **67**, 3058.

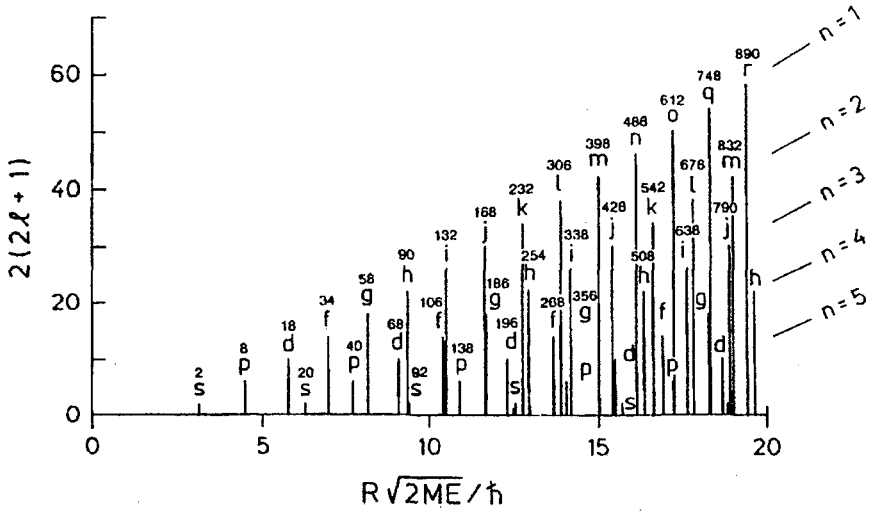

Fig. 1. The degeneracy of states of the infinitely deep spherical well on a momentum scale. The total number of fermions needed to fill all states up to and including a given subshell is indicated above each bar.

Eigenstates of the radial Schrödinger equation are often called subshells. The subshells of the infinite spherical potential well are shown ordered according to momentum in Fig. 1. The lowest energy state is 1s then comes 1p, 1d, 1f, 2p ..., etc. This is, with 2, 8, 18, 20, 34, 40, 58, 90 ... nucleons, subshells are completely filled and the corresponding nuclei could be expected to be exceptionally stable. However, these are not the observed magic numbers.

In 1949 Maria Goeppert-Mayer [1] and Haxel, Jensen and Suess [2] came up with a modified model which yielded the obseved magic numbers. Their idea was that the spin-orbit interaction is unusually strong for nucleons. Subshells with high angular momentum split and the states rearrange themselves into different groups. As we shall see the original shell model, which the nuclear physicist had to discard, describes very nicely the electronic states of metal clusters [3-18].

2 Subshells, Shells and Supershells

If it can be assumed that the electrons in metal clusters move in a spherically symmetric potential, the problem is greatly simplified. Subshells for large values of angular momentum can contain hundreds of electrons having the same energy. The highest possible degeneracy assuming cubic symmetry is only 6. So under spherical symmetry the multitude of electronic states condenses down into a few degenerate subshells. Each subshell is characterized